J Mol Model (2013) 19:1537–1551
DOI 10.1007/s00894-012-1677-8

ORIGINAL PAPER

Insights into the structural determinants for selective inhibition of nitric oxide synthase isoforms

Bruno L. Oliveira · Irina S. Moreira · Pedro A. Fernandes · Maria J. Ramos · Isabel Santos · João D. G. Correia

Received: 11 September 2012 / Accepted: 5 November 2012 / Published online: 21 December 2012

Abstract Selective inhibition of the nitric oxide synthase isoforms (NOS) is a promising approach for the treatment of various disorders. However, given the high active site conservation among all NOS isoforms, the design of selective inhibitors is a challenging task. Analysis of the X-ray crystal structures of the NOS isoforms complexed with known inhibitors most often gives no clues about the structural determinants behind the selective inhibition since the inhibitors share the same binding conformation. Aimed at a better understanding of the structural factors responsible for selective inhibition of NOS isoforms we have performed MD simulations for iNOS, nNOS and eNOS complexed with N^{ω}-NO_2-L-Arg (**1**), and with the aminopyridine derivatives **2** and **3**. The slightly better selectivity of **1** for nNOS may be assigned to the presence of extra charge–charge interactions due to its "extended" conformation. While the high affinity of **2** for iNOS can be explained by the formation of an iNOS-specific subpocket upon binding, the lack of affinity for eNOS is associated to a conformational change in Glu363. The strong van der Waals and electrostatic interactions between **3** and the active site of nNOS are most likely responsible for its higher affinity for this isoform. Owing to the elongated and narrow binding pocket of iNOS, the correct positioning of **3** over the heme group is difficult, which may account for its lower affinity toward this isoform. Brought together, our results might help to rationalize the design of selective NOS inhibitors.

Keywords Docking · Isoselectivity · Medicinal chemistry · Molecular dynamics · Nitric oxide synthase

Introduction

Nitric oxide synthase (NOS) catalyzes the O_2-dependent conversion of L-arginine to L-citrulline and nitric oxide (NO) via two consecutive reactions with N^{ω}-Hydroxy-L-arginine (L-NHA) as a stable intermediate [1]. NO is a key mammalian mediator, which, among other functions, stimulates vasodilatation in the cardiovascular system, serves as a neurotransmitter in the central nervous system, and participates in immune response by phagocytes [2].

The enzyme presents two isoforms constitutively expressed and Ca^{2+}-dependent (nNOS [neuronal NOS, NOS1] and eNOS [endothelial NOS, NOS3]), and a third isoform that is inducible and Ca^{2+}-independent (iNOS, NOS2). The enzyme is homodimeric, with each subunit containing a reductase (NOSred) and an oxygenase domain (NOSox). The NOSred domain binds flavin adenine dinucleotide (FAD), flavin mononucleotide (FMN), and the reduced form of nicotinamide adenine dinucleotide phosphate (NADPH). The NOSox domain binds the heme group, 5,6,7,8-(6R)-tetrahydrobiopterin (H_4B) cofactor and a structural zinc ion. The calmodulin (CaM) binding region, found between the two domains, regulates the reduction of NOSox by NOSred in response to Ca^{2+}-binding [1, 3]. The three NOS isoforms share about 50–60% sequence identity [2, 4].

Electronic supplementary material The online version of this article (doi:10.1007/s00894-012-1677-8) contains supplementary material, which is available to authorized users.

B. L. Oliveira · I. Santos · J. D. G. Correia (✉)
Unidade de Ciências Químicas e Radiofarmacêuticas, IST/ITN, Instituto Superior Técnico, Universidade Técnica de Lisboa, Estrada Nacional 10,
2686-953 Sacavém, Portugal
e-mail: jgalamba@itn.pt

I. S. Moreira · P. A. Fernandes · M. J. Ramos (✉)
REQUIMTE, Departamento de Química e Bioquímica, Faculdade de Ciências, Universidade do Porto, Rua do Campo Alegre s/n,
4169-007 Porto, Portugal
e-mail: mjramos@fc.up.pt

Besides mediating several physiological functions, NO overproduction by nNOS and iNOS has been reported in a number of clinical disorders including stroke, Alzheimer´s and Parkinson´s disease, cancer, septic shock, among others [5, 6]. On the contrary, NO produced by eNOS has mainly a physiological role [7–10]. Because of the double-edged nature of NO, the development of isoform-specific iNOS and nNOS inhibitors for treating NOS-related diseases is a highly desirable goal.

Several classes of potent NOS inhibitors have been reported, most of them targeting the arginine binding site of the oxygenase domain. One major class of inhibitors comprises compounds that bear a guanidine, amidino or isothiourea moiety that mimic the guanidinium group of the natural substrate [5, 11–13]. Most recently, aiming to probe NOS in vivo we have introduced a set of (radio)metal-based compounds that contain pendant L-Arg analogues [14–16]. However, the majority of the amino acid-based inhibitors exhibit poor isoform selectivity.

The high conservation of the heme active site residues of all isoforms makes the task of achieving isoform selectivity difficult (Fig. S1, Supporting information) [3]. Despite the structural homology of the active site in the three enzyme isoforms, the subtle differences found in the active pocket and in the substrate access channel are being explored for the rational design of isoform-specific NOS inhibitors. Fischmann et al. has proposed the use of larger competitive inhibitors that extend out of the binding site and explored this key active site difference to yield isoform specific inhibitors [17]. The understanding of the structural determinants responsible for isoform selectivity is fundamental for the design of potent selective inhibitors with potential clinical application. Comprehensive structure–activity relationship studies based on X-ray crystallography would allow a detailed understanding of such structural determinants. However, in the particular case of NOS, X-ray structures of known NOS inhibitors bound to all isoforms is in most cases not available and, consequently, a comparative study is not possible. Moreover, when crystals of the same inhibitor molecule bound to more than one isoform are available, the molecule often shares identical binding modes. For example, compound 1400W, a known iNOS-selective inhibitor (K_i = 7 nM for iNOS, 2 μM for nNOS, and 50 μM for eNOS), has been crystallized bound to the three isoforms, being one of the rare examples available [18]. The resulting crystal structures (iNOS: PDB code 1QW5 [19], nNOS: PDB code 1QWC [19], eNOS: PDB code 1FOI [20]) exhibit little or no differences in the active site, even 8 Å away from the ligand. The above mentioned facts, together with our interest in the design of innovative isoselective NOS inhibitors based on metal complexes, [15] prompted us to study the binding of known NOS inhibitors by molecular dynamics simulations. We have chosen Nitro-L-arginine (N^{ω}-NO_2-L-Arg, **1**), which is a well-known inhibitor of NOS with poor NOS isoselectivity. For comparison, we have also chosen the selective iNOS inhibitor **2** (4-({4-[(4-methoxypyridin-2-yl)amino]piperidin-1-yl}carbonyl)-benzonitrile) and the selective nNOS inhibitor **3** (N-{(3R,4R)-4-[(6-amino-4-methylpyridin-2-yl)methyl]pyrrolidin-3-yl}-N'-[2-(3-fluorophenyl)ethyl]ethane-1,2-diamine) (Table 1) [21, 22]. In the latter case, we chose the isomer **3**-(3*R*,4*R*) as it is much more potent and selective than the other isomers [21]. Inhibitors **2** and **3**, which belong to the aminopyridine family, were developed using structure-based drug design methods. They are included in the new class of inhibitors that extends out of the binding site where the structural differences among the three isoforms are more evident [21].

The work presented herein aims to provide insights into the binding modes and affinity of **1** – **3** to the NOS isoforms using computational methods. The starting coordinates for molecular docking and molecular dynamics (MD) simulations were taken from the X-ray structures of iNOS, nNOS and eNOS isoforms with the PDB codes 1QW4, 1ZVL, and 1D1W, respectively. In the case of the complexes that have crystal structures (**1**:nNOS, **1**:eNOS, **2**:iNOS, **3**:nNOS and **3**:eNOS) the AutoDock software was able to correctly reproduce the experimental structures. Starting from the docked conformations MD simulations were further performed to better investigate the micro-environment of the binding pocket. As no tridimensional structure exists for the complexes **1**:iNOS, **2**:nNOS, **2**:eNOS and **3**:iNOS the validated docking protocol was combined with MD simulations

Table 1 NOS inhibitors **1** – **3** and experimental inhibition constants

Compound	Inhibition constants		
	iNOS	nNOS	eNOS
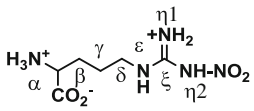 **1**	3.1[a]	0.29[a]	0.35[a]
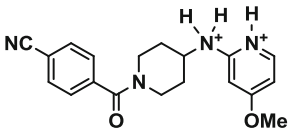 **2**	0.074[b]	6[b]	> 100[b]
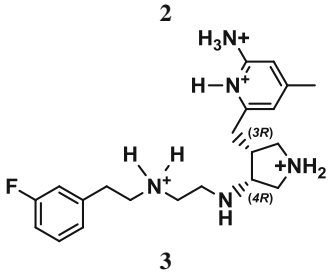 **3**	3.9[c]	0.005[c]	20.3[c]

[a] K_i values (μM) taken from [23]

[b] IC50 values (μM) taken from [22]

[c] K_i values (μM) taken from [21]

to rationally predict the binding mode of the inhibitors **1 – 3** in the correspondent NOS isoforms and to understand their structural differences. The analysis of the structural ensemble generated by MD simulations complements high-resolution X-ray crystal structures data and can provide additional knowledge about the most important molecular interactions, which is a key issue for the design of novel potent isoselective inhibitors.

Materials and methods

Docking and MD simulations

AutoDock4.2 was employed to perform protein-ligand docking calculations. The protein structures were taken from the Research Collaboratory for Structural Bioinformatics (RCSB) protein database. The best quality structures, with the highest resolution and intact X-ray structure, were chosen among all PDB structures of the NOS isoforms (chain A of PDB 1QW4 for iNOS [19], 1ZVL for nNOS [23] and 1D1W for eNOS [24]). The solvent molecules were removed, but the heme and H_4B were retained. The 3D-structures of the ligands were extracted from the PDB structures. The protein-ligand complexes were prepared with AutoDockTools: for each protein hydrogen atoms were added and Kollman united atom charges were assigned. Hydrogens were also added to the ligands, heme and H_4B, and charges were calculated by the Gasteiger-Marsili method. The Fe atom of heme was assigned a charge of +3. The rotatable bonds in the ligands were assigned with AutoDockTools and are depicted in Fig. S2. The ligands were docked inside a cubic grid box (48 Å × 32 Å × 58 Å) centered on the Fe atom of the heme group with a grid spacing of 0.375 Å. In each docking simulation 100 independent Lamarckian genetic algorithm (LGA) runs were performed, with the population size set to 200, the number of energy evaluations set to 10,000,000 and the maximum number of generations set to 27,000. All other parameters were maintained at their default settings [25, 26]. The resulting docked orientations within a RMSD of 2 Å were clustered together. The lowest and more populated energy cluster returned by AutoDock that fulfilled some known structural criteria important for enzyme activity was used for conformational binding analysis. RMSD between the experimental and computational structures of the inhibitors were computed to evaluate the accuracy of the calculated poses [**1**:nNOS(1K2R) and **1**:eNOS(8NSE); **2**:iNOS(3EAI); **3**:nNOS(3JWT) and **3**:eNOS(3JWX)]. These structures obtained by docking were then subjected to a final refinement using MD simulations with explicit water. In the case of the inhibitor:NOS complexes for which no X-ray structures are available (**1**:iNOS; **2**:nNOS and **2**:eNOS; **3**:iNOS), the validated docking protocol was used combined with MD simulations to predict the binding modes of the inhibitors. Starting from the X-ray structures of iNOS (PDB 1QW4), nNOS (PDB 1ZVL) and eNOS (PDB 1D1W) the complexed ligands were removed and the resulting structures were used to simulate the unbound isoforms. The protonation state of the inhibitors **1 – 3** at physiologic pH was determined with Epik 1.6 (Schrödinger) [27]. Partial atomic charges for **1 - 3** were derived by optimizing their geometries and calculating electrostatic potentials at the HF/6-31G* level of theory and then fitting charges to these potentials using the RESP method, [28, 29] as implemented in R.E.D. Server 2.0 [30–32]. A detailed description of this procedure is reported in Fig. S3. The topologies and parameters of the inhibitors compatible with the CHARMM all atoms force field were derived from the ParamChem server (https://www.paramchem.org/) [33].

The three isoforms exist as dimers with a structural Zn^{2+} ion coordinated by four cysteines, two cysteines from each monomer (Cys104 and Cys109 in iNOS, Cys326 and Cys331 in nNOS, Cys96 and Cys101 in eNOS). Keeping in mind that the Zn^{2+} ion is 22 Å away from the active center, and has no effect on the substrate binding, it has been excluded from the simulation. Moreover, Li et al. have shown experimentally that in the absence of Zn^{2+} ion, the symmetry related cysteines form a disulfide bridge [34].

To increase length of the simulations without losing important structural information, only one oxygenase monomer was selected. To investigate if the simulation of only one monomer affects the interactions of the inhibitor with the protein we performed comparative MD simulations of **3** bound to nNOS and eNOS in the monomeric (**3**:nNOS and **3**:eNOS) and dimeric forms (**3**:$nNOS_{dimer}$ and **3**:$eNOS_{dimer}$). MD simulations of the monomeric forms were performed with positional constraints on the H_4B to keep this co-factor fixed in its X-ray position, while in the case of the dimeric forms fully unconstrained simulations were performed.

The 15 simulations were performed using NAMD [35] and the CHARMM27 force field [36]. VMD version 1.8.7 was used for trajectory analysis [37]. The oxo-ferryl form (compound I) of heme, which has an oxygen atom at the sixth coordination position of iron, was used. The force field parameters of the H_4B cofactor and compound I were kindly provided by Cho et al [38]. The propKa module of the PDB2PQR server (http://kryptonite.nbcr.net/pdb2pqr/) was used to adjust the protonation states of ionizable residues at physiological pH [39–41]. Water molecules observed in the crystals structures were kept and additional TIP3P water molecules (box of dimension 10 Å x 10 Å x 10 Å) were modeled using the solvate package in VMD. Next, the systems were neutralized by adding counter ions with the autoionize package in VMD. The whole systems contained: **unbound iNOS** - 418 residues, 18,319 water molecules and

9 Na^+ (61,723 atoms total); **unbound iNOS$_{dimer}$** - 836 residues, 40,251 water molecules and 18 Na^+ (13,4395 atoms total). **unbound nNOS** - 419 residues, 17,049 water molecules and 3 Na^+ (57,798 atoms total); **unbound eNOS** - 414 residues, 16,850 water molecules and 2 Na^+ (57,176 atoms total); **1:iNOS** - 418 residues, 17,132 water molecules and 5 Na^+ (58,281 atoms total); **1:nNOS** - 419 residues, 17,050 water molecules and 2 Na^+ (57,829 atoms total); **1:eNOS** - 414 residues, 16,851 water molecules and 1 Na^+ (57,207 atoms total); **2:iNOS** - 418 residues, 18,685 water molecules and 5 Na^+ (62,978 atoms total); **2:nNOS** - 419 residues, 17,939 water molecules and 1 Na^+ (60,514 atoms total); **2:eNOS** - 414 residues, 18,138 water molecules and 4 Na^+ (60,880 atoms total); **3:iNOS** - 418 residues, 17,039 water molecules and 2 Na^+ (58,020 atoms total); **3:nNOS** - 419 residues, 17,938 water molecules and 1 Cl^- (60,524 atoms total); **3:nNOS$_{dimer}$** - 838 residues, 29,690 water molecules and 5 Na^+ (102,484 atoms total); **3:eNOS** - 414 residues, 18,137 water molecules and 2 Na^+ (60,888 atoms total); **3:eNOS$_{dimer}$** - 828 residues, 30,735 water molecules and 7 Na^+ (122,147 atoms total).

All models were subjected to 3000 energy minimization steps and then simulations continued for another 8 ns. Rigid bonds were used for all hydrogen atoms, thus allowing a time step of 2 fs to be used. The force field parameters were kept standard as specified by the CHARMM force field. Short range nonbonded van der Waals interactions were computed every 2 fs, and the long-range electrostatic ones were computed every 4 fs. Starting from a switching distance of 10 Å, the Lennard-Jones potential was smoothly reduced to zero at a cutoff distance of 12 Å. The particle mesh Ewald (PME) method was employed for full electrostatics, with a grid point density of at least $1/Å^3$ in all cases [42]. The simulations were performed in the NPT ensemble, using the Nosé–Hoover Langevin piston method for pressure control (1 atm), with an oscillation period of 200 fs and a damping time of 50 fs; constant temperature (T = 310 K) was enforced using Langevin dynamics with a damping coefficient of 5 ps^{-1} on all nonhydrogen atoms [43–46]. Harmonic constraints were used to restrain the H_4B cofactor to its crystallographic position with a harmonic force of 0.3 kcal mol^{-1}.

Several detailed analyses were carried out for the trajectories obtained from the last 4 ns of the equilibrated simulations. The NAMD energy plugin of VMD was used to calculate the electrostatic interaction energies between protein and inhibitors for each snapshot of the MD trajectory. The water molecules, which were within 3 Å from the inhibitors in each snapshot were identified by using appropriate Tcl script executed within VMD, and the percentage of residence time calculated. The averaged-structures of the last 4 ns of the simulations were also calculated using appropriate Tcl script. All the pictures were made with the Pymol software [47].

Computational details for VolArea

All calculations were done with a box volume of 24.9 Å, 23.1 Å and 14.2 Å centered on the heme group. The resolution used for volume calculation was 1.0 $Å^3$ [48].

Computational details for travel depth

Travel depth allows the measurement of the depth of the molecular surface for examining pockets and ligand binding sites as well as the overall depth of the surface. In this software [49], travel depth is defined as the minimum distance from any surface point to the convex hull avoiding the protein interior, and is calculated using the multiple source shortest paths (MSSP) algorithm [50].

Results and discussion

Docking

The AutoDock software was used to dock **1** into iNOS, **2** into nNOS and eNOS, and **3** into iNOS since no X-ray structures exist for such inhibitor:protein complexes. 3D structural information of the target proteins were taken from the PDB entries 1QW4 (iNOS), 1ZVL (nNOS) and 1D1W (eNOS) because of their reasonable resolution (2.0 – 2.5 Å) and intact X-ray structures.

The most straightforward method to validate the accuracy of a docking procedure is to determine how closely the lowest energy conformation predicted by the scoring function of the docking software compares with the bound conformation of the experimental X-ray structure. The docking procedure was validated by redocking **1** inside the active pocket of nNOS and eNOS, **2** inside the active pocket of iNOS and **3** inside the active pocket of nNOS and eNOS. In a general way, the docking solutions reproduced the binding modes observed experimentally. In the case of **1** we found a good agreement between the docked and experimental conformations with RMSDs of 2.82 Å and 2.61 Å for **1**:nNOS and **1**:eNOS, respectively (Fig. 1a and b).

In Fig. 1c is shown the predicted conformation of **1** inside the iNOS binding pocket. The lowest-energy conformations of this inhibitor in all isoforms were found to have identical binding orientations: the NO_2-guanidine group is placed over the Fe-O atoms of the heme co-factor anchored by Glu residue while its amino-acid function is hydrogen-bonded to the heme propionate A and Gln residue (Fig. 1a – c).

In the **2**:iNOS complex the inhibitor adopted a conformation close to the one found in the crystal structure. The aminopyridine core is anchored by bidentate H-bonds to Glu371 of the active site, and the rigid tail is extended above the heme propionate arms (Fig. 1d). The RMSD found

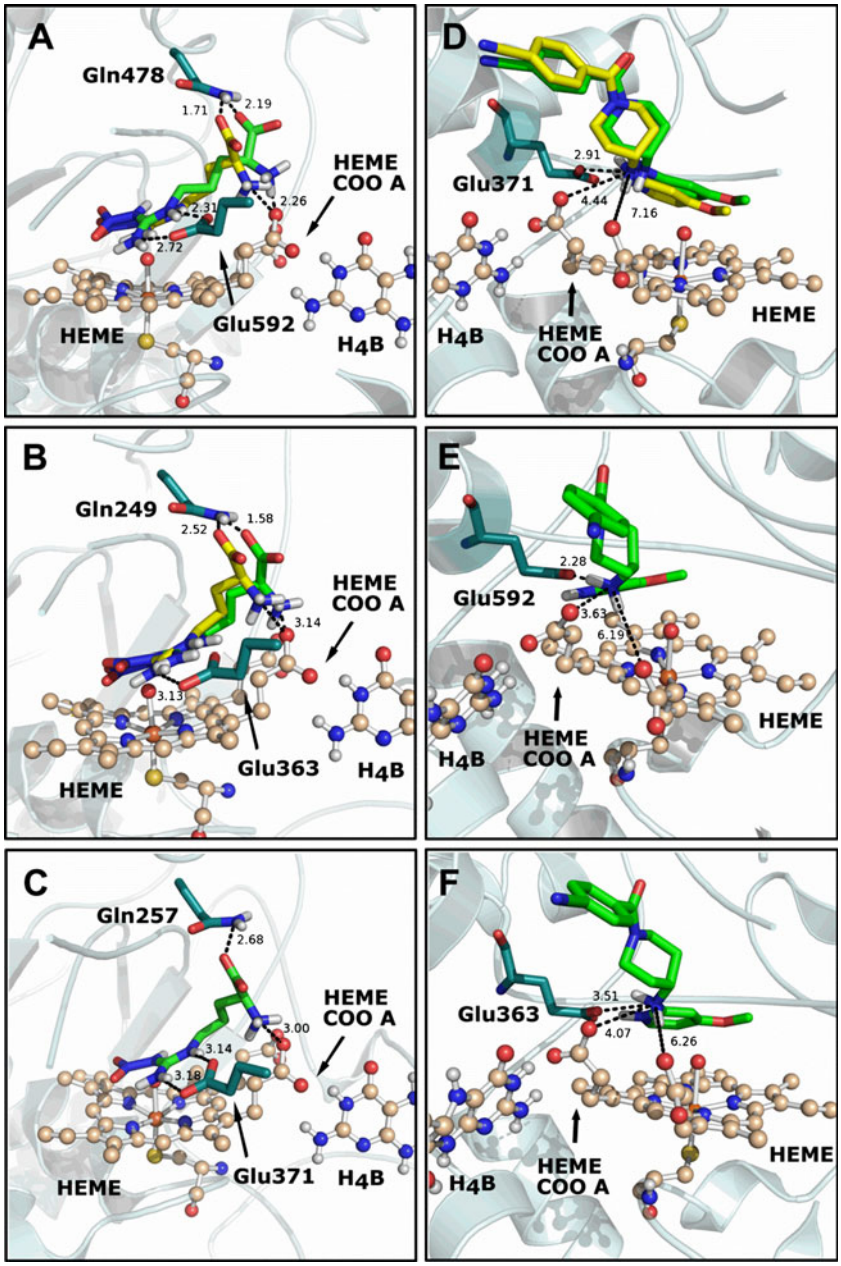

Fig. 1 Lowest energy binding conformations of **1** inside nNOS (**a**), eNOS (**b**) and iNOS (**c**), and **2** inside iNOS (**d**), nNOS (**e**) and eNOS (**f**). Inhibitors **1** and **2** are shown in green sticks (predicted binding pose) or in yellow sticks (X-ray binding pose). The heme and H_4B co-factors are shown in ball and stick representation. All nitrogen atoms are blue, oxygen atoms are red, sulfur atoms are yellow and iron is orange. Only polar H-atoms are shown for clarity. The same representation will be used in the following figures

between the docked ligand and the X-ray structure was 1.42 Å. Docking experiments performed for **2**:nNOS and **2**:eNOS indicated that in the lowest-energy conformation **2** binds to both isoforms (Fig. 1e and f) in a similar way to what was observed in the X-ray structure of **2**:iNOS.

Docking calculations for **3**:nNOS has shown that the predicted position has some differences compared to the one found in the X-ray structure. The fluorophenyl packs less parallel to the heme plane and the aminopyridine group interacts with Gln478 and Ser477 instead of making bifurcated H-bonds with the heme propionate D (Fig. 2a, green sticks). A closer inspection of the X-ray structure of the nNOS isoform used in the docking (PDB code 1ZVL) revealed that Tyr706 is rotated and points out to the heme propionate D (Fig. 2a).

This subtle difference in the orientation of this residue is a key issue. In fact, this residue sterically blocks the interaction between the aminopyridine group of **3** and the heme propionate D. It is therefore not surprising the difficulty in achieving a more accurate docking result. It should be mentioned that the coordinates used as a template for all docking studies with nNOS were taken from the X-ray structure of L-Arg bound to this isoform. As this inhibitor is not large enough to reach the region of Tyr706, the side chain of this residue has space to be accommodated near the heme propionate D, blocking in this way a possible interaction with the heme arm. We tried to overcome this issue by adding flexibility to Tyr706, which has not been taken into account before because it is too far from the active site.

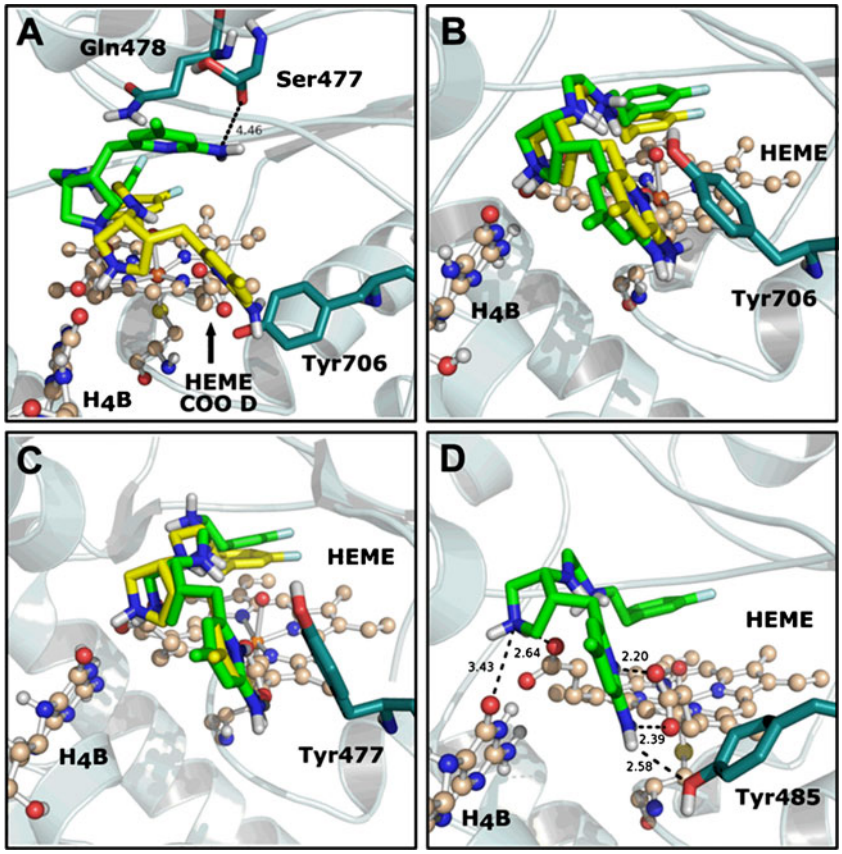

Fig. 2 Predicted binding mode of **3** inside the active site of nNOS (**a** and **b**), eNOS (**c**) and iNOS (**d**). Inhibitor **3** is shown in green sticks (predicted binding pose) or in yellow sticks (X-ray binding pose). Only polar H-atoms are shown for clarity

From this docking, we obtained a binding conformation that, when compared with the conformation of **3** found in the X-ray structure, was very similar (Fig. 2b, RMSD 1.35 Å). The binding mode resulting from these docking studies has been termed the "flipped" binding mode by Delker et al. [51]. In the "normal" binding mode, the aminopyridine moiety interacts with the Glu residue of the active site and is stacked over the heme group. This ambiguity in the binding mode of **3** was reported by the same authors, which suggested that the inhibitor chirality [**3**-(3*R*,4*R*), **3**-(3*R*,4*S*), **3**-(3*S*,4*S*) and **3**-(3*S*,4*R*)] controls the orientation of **3** inside the active pocket of nNOS [51]. It is worth mentioning that in docking studies performed considering inhibitor **3** fully flexible (except the ring systems) we also obtained low energy conformations that reproduced the "normal" binding mode. As all bonds were set to be treated as flexible the docking algorithm allowed for switching between chiral forms, which justified the obtained results. In the case of **3**:eNOS, the conformation with minimum energy showed that **3** bounds eNOS with its aminopyridine moiety hydrogen-bonded to the side chain of Glu363, the so called "normal mode" (Fig. S4). In the docked conformation of another low ranked cluster, inhibitor **3** displayed a binding mode similar to that found in the X-ray structure, with the fluorophenyl situated over the heme (Fig. 2c, RMSD 1.48 Å). Docking calculations for **3**:iNOS yielded one highly populated cluster with the inhibitor bound in the "flipped" binding mode (Fig. 2d).

Molecular dynamics

Analysis of the trajectories

With the aim of rationalizing the binding mode of **1** – **3** inside the binding pocket of the NOS isoforms as well as the conformational changes induced in the isoforms by the binding of the different inhibitors, we performed MD simulations of the three isoforms in the presence and in the absence of **1** – **3**. Useful simulations for large systems like the NOS homodimer are quite expensive and time consuming. Therefore, to increase length of the simulations without losing important structural information, only one oxygenase monomer was selected. In a first set of simulations we observed that H_4B co-factor was not stable at the position of the crystal structure and, despite being tightly bound to the heme propionate A by strong H-bonds, the H_4B co-factor drifts from its X-ray position after ~1.5 ns (Fig. S5). Having in mind that the H_4B is located near the dimer interface, it was necessary to apply light constraints on the position of the H_4B co-factor for all MD simulations. Previously published MD simulations performed with iNOS and eNOS isoforms complexed with L-Arg were done without restrains on the H_4B co-factor [52]. In this study the drift of H_4B was not observed, most likely because their simulations only run for 1.0 ns. In our case, after 1.5 ns the system was not yet stable and fully relaxed, and longer

simulations with the H_4B co-factor restrained were needed. To investigate the effect of simulating only one monomer we performed comparative MD simulations of the monomeric and dimeric unbound iNOS (in the absence of inhibitor). To clarify if the binding of the inhibitors is influenced by the use of only one monomer we performed MD simulations of **3** bound to nNOS and eNOS in the monomeric (**3**:nNOS and **3**:eNOS) and dimeric forms (**3**:$nNOS_{dimer}$ and **3**:$eNOS_{dimer}$). Our results indicate that the dynamics of the monomer and dimer were similar (Fig. S6). It is important to highlight that in the case of the fully unconstrained simulations of the dimeric forms the H_4B co-factor is stable in its X-ray position.

Structural stability during MD simulations

The backbone RMSD values with respect to the initial structures were calculated along the 8 ns of the trajectories to assess the stability of the three NOS isoforms during the MD simulations. For the sake of example, the RMSD values for the unbound iNOS, nNOS and eNOS isoforms are shown in Fig. 3.

The RMSDs of the unbound isoforms remain stable after an initial period of equilibration, oscillating around ~1.5 - 3.5 Å during the simulation time. The RMSDs reach the plateau at ~3.5 ns indicating that 8 ns simulation is enough for stabilizing the fully relaxed systems. The RMSD of the isoforms iNOS, nNOS and eNOS complexed with the inhibitors **1** – **3** also demonstrated the stability of the models. As an example, the RMSD values of the NOS isoforms complexed with **1** as a function of time for the 8 ns of simulation is shown in Fig. S7a . The RMSD values of the inhibitors versus simulation time were also checked. These results indicate that **1** – **3** appear to have been stabilized in all cases after an initial period of equilibration. As an example Fig. S7b shows the RMSD values of **1** during the simulation time.

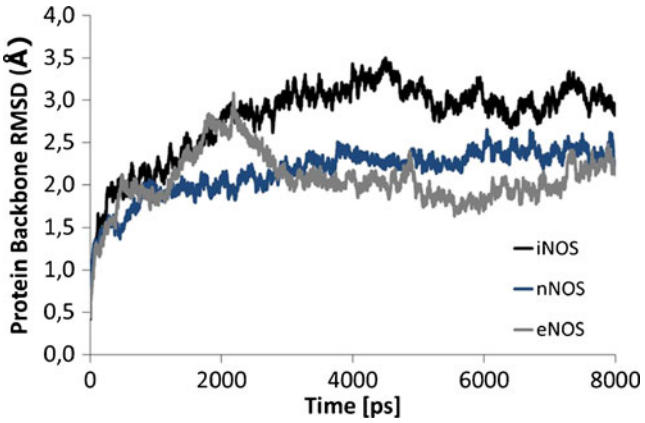

Fig. 3 Overall RMSD of the protein backbone over 8 ns simulation is shown for the unbound iNOS (*black*), nNOS (*blue*) and eNOS (*grey*) isoforms

MD simulations of the unbound NOS isoforms

MD simulations of the unbound isoforms starting from the X-ray structures without the ligands were performed to study conformational changes in the active site region of the enzyme. Figure S8 shows the structural micro-environment around the active site of the unbound isoforms after MD simulation.

To assess the main differences within the binding pocket the VolArea software was used to calculate their volume, and the travel depth computed to predict their ligand binding cavities. The volumes of the active site cavities for the unbound iNOS, nNOS and eNOS isoforms were 1182.0 ± 1.6 $Å^3$, 2203.0 ± 8.2 $Å^3$ and 2489.0 ± 7.7 $Å^3$, respectively (Fig. 4a – c). The mean travel depth for all atoms in each NOS isoform is depicted in Fig. 4d – f. The travel depth of iNOS isoform is significantly higher than that of the other isoforms, indicating that the binding cleft is further away from the surface (Fig. 4d – f). These results show that the active site of iNOS presents a deeply buried smaller binding pocket, which suggests relevant differences between iNOS and nNOS/eNOS in terms of binding. Unlike the binding site of nNOS/eNOS, which is "more open", the binding site of iNOS seems to be less prone to accommodate larger groups. This difference is most likely an important issue for isoselectivity achievement.

Overall interactions of NOS with inhibitors 1 – 3

Binding mode of 1 in NOS isoforms

The X-ray structures of both nNOS (PDB ID 1K2R) and eNOS (PDB ID 8NSE) isoforms in complex with **1** demonstrated that the inhibitor shares identical binding modes with almost superimposable structures (RMSD = 0.261 Å, Fig. S9). To identify molecular determinants that could explain the different affinities of **1** for the three isoforms we performed MD simulations for the complexes **1**:iNOS, **1**:nNOS and **1**:eNOS. Our simulations revealed that **1** is anchored in the active site of NOS through a bidentate interaction between the nitrogen atoms (Nε, Nη1; see Table 1 nomenclature and Table S1 for distances) of the NO_2-guanidine moiety and the oxygen atoms of the CO_2^- of the Glu residue (Glu371:iNOS; Glu592:nNOS; Glu363:eNOS) (Fig. 5a). The H-bonds involved in this interaction are relatively short and comparable for all three isoforms (e.g., distance between Glu371:OE1 and $N\eta_1$:NO_2Arg = 2.69 ± 0.08 Å in **1**:iNOS; dist. Glu592:OE1····$N\eta_1$:NO_2Arg = 2.74 ± 0.09 Å in **1**:nNOS; dist. Glu363:OE1····$N\eta_1$:NO_2Arg = 2.78 ± 0.22 Å in **1**:eNOS; **Table S1**). This critical H-bonding network plays a crucial role in the catalytic activity by placing substrates or inhibitors of NOS over the heme unit. Additionally, the Nη1 atom H-bonds to the backbone

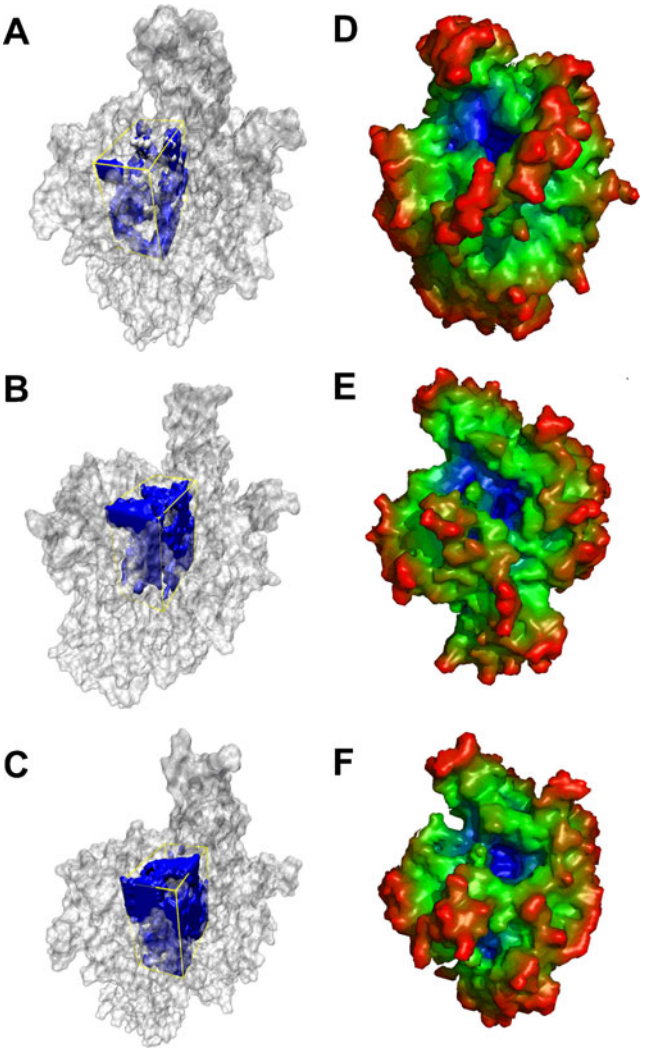

Fig. 4 Surface representations of the unbound iNOS (**a**), nNOS (**b**) and eNOS (**c**) isoforms. The volumes of the active site cavities for the isoforms are represented in blue. All calculations were done with a box volume of 24.9 $Å^3$, 23.1 $Å^3$ and 14.2 $Å^3$ centered on the heme group. The resolution used for volume calculation was 1.0 $Å^3$. The right panel shows the travel depth of the three unbounds NOS isoforms, iNOS (**d**), nNOS (**e**) and eNOS (**f**). The molecular surface is colored by increasing travel depth from red to green to blue

carbonyl of Trp (distance between Trp366:C=O and Nη1:NO_2Arg = 2.96 ± 0.20 Å in **1**:iNOS; dist. Trp587:C=O····Nη1:NO_2Arg = 2.03 ± 0.16 Å in **1**:nNOS; dist. Trp358:C=O····Nη1:NO_2Arg = 2.85 ± 0.17 Å in **1**:eNOS).

The different affinities of **1** for the three isoforms may be explained by small changes in the position of the α-amino-acid group (Fig. 5). The better affinity of **1** for nNOS results from the "extended" conformation adopted by the inhibitor, which is stabilized by an interaction observed between the –CO_2^- group of **1** and the Arg481 (Fig. 5b). This interaction, absent in the complex **1**:iNOS, can be explained based on the mutation of Asn498 in nNOS that is Thr277 in iNOS. The Asn498 is situated in the substrate access channel, relatively far from the binding site. However, the side-chain of Asn498 in nNOS is interacting with the Arg481, inducing a rotation in this residue that place its side-chain in position to interact with the –CO_2^- group of the inhibitor (distance between Arg260:NH1and CO1:NO_2Arg = 5.31 ± 0.32 Å in iNOS;dist. Arg481:NH1···· CO1:NO_2Arg= 2.82 ± 0.21 Å in nNOS). In the complex **1**:iNOS this interaction does not exist, and consequently, the inhibitor adopts a "curled" conformation that place its –CO_2^- group close to the –CO_2^- of the Asp 376 residue (distance between Asp376:OD1 and CO1:NO_2Arg = 3.81 ± 0.32 Å in iNOS; dist. Asp597:OD1····CO1:NO_2Arg = 7.37 ± 0.57 Å in nNOS), resulting in electrostatic repulsion. For each MD trajectory we used the NAMD energy plugin in VMD to calculate the interaction energies between **1** and the residues Asp376/Asp597 and Arg260/Arg481 in iNOS and nNOS, respectively [37]. Dissection of the energetics shows that the nonbonded electrostatic interaction between **1** and the Asp376 residue in iNOS is 16.61 ± 4.73 kcal mol^{-1}, while the electrostatic energy for the "same interaction" in nNOS is -6.43 ± 4.21 kcal mol^{-1}. Moreover, the energy contribution due to Arg260 (-30.28 ± 10.21 kcal mol^{-1}) in iNOS was smaller than that due to Arg481 (-60.09 ± 6.31 kcal mol^{-1}) in nNOS. The more favorable energetic interaction between **1** and nNOS is a plausible explanation for the higher selectivity to this isoform over iNOS.

The simulation results also indicate that inhibitor **1** shares an identical binding mode in iNOS and eNOS (Fig. 5a, green and yellow sticks). The better affinity of **1** for eNOS over iNOS could be justified based on the mutation of Asn368 in eNOS that is Asp376 in iNOS. In this way, the previous destabilizing interaction observed between the CO_2^- group of **1** and the electronegative environment created by Asp376 is not present. Consequently, in **1**:eNOS the inhibitor adopts the "curled" conformation to place the α-CO_2^- group in position for maximum electrostatic stabilization with the Asn368.

Since water molecules can play an important role in ligand binding, water-mediated interactions between **1** and the three NOS isoforms were checked (Fig. 6).

In the complex **1**:iNOS two intercalated water molecules (W1 and W2), with residence times of 100 % during the last 4 ns of simulation, were found between the -CO_2^- group of **1** and Asp376 and Tyr 367, establishing a H-bond network between the inhibitor and these two residues (Fig. 6a). A third water that do not exchange and persist throughout the last 4 ns was observed near the Nη2-atom of the NO_2-guanidine moiety (Fig. 6a, W3). This conserved water molecule is also observed in the complexes **1**:nNOS and **1**:eNOS (Fig. 6b, **W2** and Fig. 6c, **W1**). An equivalent water molecule can be found in the X-ray structures of nNOS and eNOS crystallized with N^{ω}-NO_2-L-Arg (PDB code 1K2R, chain A HOH1867 and PDB code 8NSE, chain A HOH1047). One additional

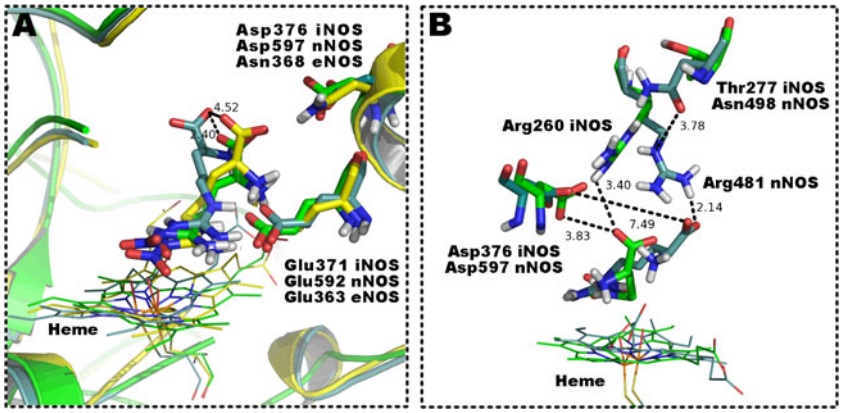

Fig. 5 **a** Alignment of the average structures of **1**:iNOS, **1**:nNOS and **1**:eNOS calculated using the last 4 ns of simulation. Inhibitor **1** is shown in green (iNOS), deep teal (nNOS) and yellow (eNOS) sticks. **b** Binding mode of **1** in iNOS and nNOS. In complex **1**:nNOS, **1** adopts an "extended" conformation that is stabilized by Arg481, which is hydrogen-bonded to Asn498

water molecule was observed trapped at the interface of the complex **1**:nNOS, occupying 100 % of the simulation time, mediating an interaction between the O-atom of Asp597 and the Nε-atom of the NO_2-guanidine moiety of **1** (Fig. 6b, W1).

Binding mode of 2 in NOS isoforms

Inhibitor **2** binds similarly to the active site of iNOS and nNOS, with the aminopyridine moiety making bidentate H-bonds with the Glu residue (Glu371:iNOS; Glu592:nNOS; Glu363:eNOS), mimicking the interactions of the guanidinium group of L-Arg (Fig. 7a and b).

The interaction with Glu anchors the aminopyridine moiety almost parallel to the heme plane and places the bulky cyanobenzyl unit extended above the heme propionate arms, packing with the residues Gln (Gln257:iNOS; Gln478:nNOS) and Arg (Arg260 and Arg382 in iNOS; Arg481 and Arg603 in nNOS) (Fig. 7a and b). In the case of the complex **2**:eNOS (Fig. 7c) the positioning of the aminopyridine moiety of **2** over the heme group is not observed, which may account for its lower affinity toward this isoform.

Aimed at a better visualization of the structural rearrangements in the active site of NOS induced by **2**, Fig. 8 displays both the X-ray (black lines) structures and the structures obtained after MD refinement (deep teal sticks).

The most likely reason for the 80-fold selectivity to iNOS over nNOS is the enhanced hydrophobic and cation-π interactions of the cyanophenyl group of **2** with Arg260 and Arg382 of iNOS. In fact, the "so-called" Gln-opened conformation accounts for the observed isoselectivity by helping in the orientation of the cyanophenyl group near the residues Arg260 and Arg382 (Fig. 8b and Fig. S10). The rotation from the Gln-closed conformation (Fig. 8a) to Gln-opened conformation (Fig. 8b), is induced by the inhibitor binding, as can be concluded by comparison with the MD simulation of the unbound iNOS.

This induced conformation of the Gln257 promotes the rotation of Arg260, which in turn is stabilized by a H-bond with Thr277 (Asn498 in nNOS and Asn269 in eNOS). This behavior was also recently reported by Garcin et al., who demonstrated that some ligands were able to promote a rotation of Gln257 residue and, therefore, to open an iNOS-specific subpocket that might be important for isoform specific ligand design [22].

In **2**:nNOS the "closed-conformation" is promoted by the H-bonding between Gln and Tyr588 (Fig. 8c). The closed conformation in nNOS and eNOS could also be ascribed to the bulkier Asn498/Asn269 residues (Fig. 8b – d). Due to steric hindrance, Arg481 and Arg252 residues in nNOS and eNOS, respectively, are forced to shift, while the corresponding and less bulky Thr277 in iNOS does not have the same effect in Arg260 residue. The shift in Arg252 in the complex **2**:eNOS is even more pronounced due to the presence of the bulkier residues Ile272 and Leu291 (compared to Phe280 and Leu299 in iNOS and Phe501 and Leu520 in

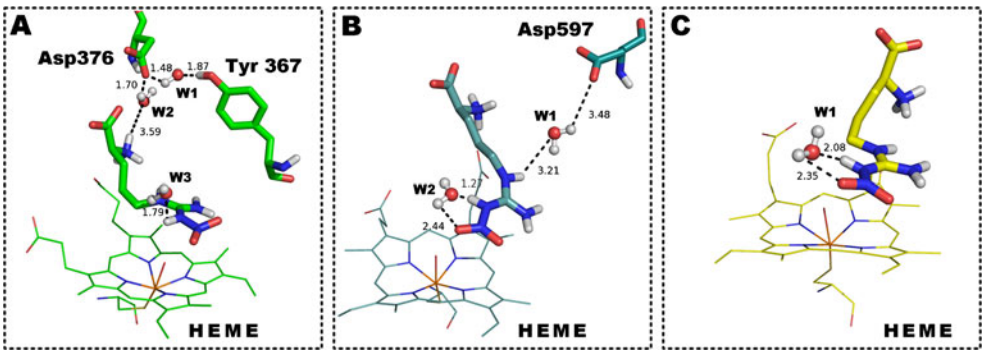

Fig. 6 Conserved water molecules and water-mediated interactions in the simulation of the complexes **1**:iNOS (**a**), **1**:nNOS (**b**) and **1**:eNOS (**c**). Water molecules are shown in ball and stick representation and present residence times of 100 % (calculated considering the last 4 ns of the simulation)

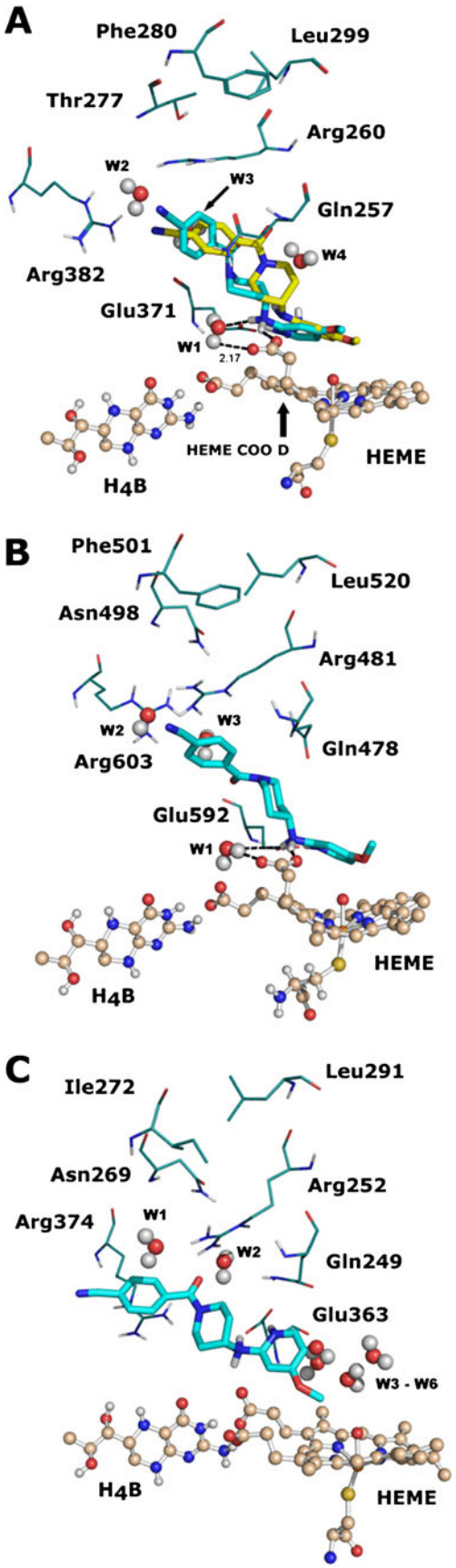

◀ **Fig. 7** Structural micro-environment around the active site of **2**:iNOS (**a**), **2**:nNOS (**b**) and **2**:eNOS (**c**) complexes. Inhibitor **2** is shown in cyan sticks (representative conformation obtained from MD simulation) or in yellow sticks (X-ray binding pose).

nNOS). The effect of the bulkier residues in **2**:eNOS have a great influence in the inhibitor-binding orientation. In fact, the inhibitor is not planar, as is the case in the other two isoforms, which leads to the loss of the inhibitor-heme π-stacking interaction. Such situation is most likely the justification for its lower affinity toward eNOS. Indeed, previous studies have demonstrated that a planar system accounts for improved affinity compared to a nonplanar system [53]. The low affinity of inhibitor **2** to eNOS could also be explained based on an energetic penalty associated to the observed conformational change of Glu363 (Fig. 8d). Such change has already been described by Rosenfeld et al., who studied a nitroindazole-derived family of NOS inhibitors, which induced a conformational change in Glu as concluded by X-ray structural studies [53]. Comparison of the experimental binding affinities of the inhibitors for wild-type iNOS with those determined for mutant E371A allowed to conclude that there was an energetic penalty of about 1–2 kcal mol^{-1} associated to this conformational change [53]. It is worth mentioning that this conformational mobility of Glu363 was not observed in the simulation of the complex **1**:eNOS.

There are a number of water molecules participating in direct interactions with the inhibitor **2** and the three NOS isoforms. In the case of **2**:iNOS four water molecules with residence times of 99.6 % (W1), 97.67 % (W2), 85.91 % (W3) and 56.45 % (W4) were found trapped at the interface inhibitor:protein (Fig. 7a). In **2**:nNOS the three water molecules placed near the inhibitor have residence times of 100 % (Fig. 7b, W1 – W3). One of these conserved water molecules (W1), common to both **2**:iNOS and **2**:nNOS systems, acts as a bridge between the N atom of the pyridine amine ring and the heme propionate D. In **2**:eNOS the water molecule interaction described previously is not present and this can be a possible justification for inhibitor displacement (Fig. 7c).

Binding mode of 3 in NOS isoforms

The binding mode of **3** in nNOS is consistent with the binding mode found in the X-ray structure (Fig. S11). The inhibitor binds with the fluorophenyl group positioned over the heme plane in a co-planar and almost parallel conformation, maintaining the stacking interactions during the entire simulation (Fig. 9a). The nitrogen atom of the pyrrolidine ring forms favorable H-bonds with heme propionate A, as well as with O4 atom of H_4B. The nitrogen atom of the ethylenediamine fragment is involved in electrostatic interactions with Glu592. The aminopyridine is also making favorable π-stacking interactions with the Tyr706.

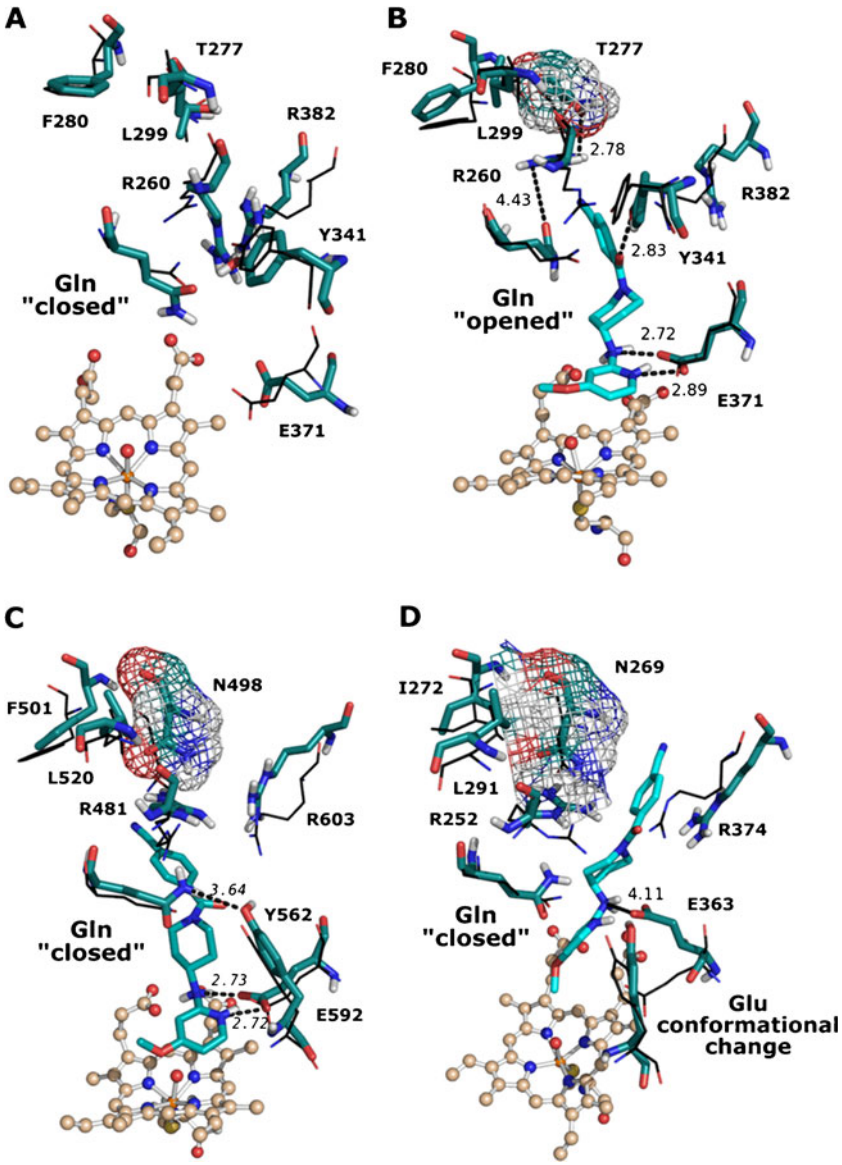

Fig. 8 Structural micro-environment around the active site of iNOS unbound (**a**), **2**:iNOS (**b**), **2**:nNOS (**c**) and **2**:eNOS complexes (**d**). Initial and MD structures are shown in black lines and deep teal sticks, respectively. In iNOS the rotation of Gln257 and Arg260 (stabilized by a H-bond with T277) opens the Gln specificity pocket for binding of the bulky inhibitor tail (**a** and **b**). Bulky Asn498/Asn269 residues in nNOS/eNOS induced a shift in the Arg481 and Arg252 residues, which prevent the opening of the specific pocket (**c** and **d**). In **2**:eNOS the inhibitor is not planar to the heme. Conformational change observed in the Glu363 residue in eNOS should have a great influence in the inhibitor-binding orientation (**d**)

The binding mode of **3** in eNOS is very similar to that described for **3**:nNOS. Indeed, the molecule binds almost in the same position in both isoforms. The 2600-fold nNOS selectivity of **3** over eNOS can be explained based on the conformational change of the side chain of Glu363, similar to the one observed for **2**:eNOS. Our results revealed that after 100 ps of simulation the side chain of Glu363 adopts an alternate conformation (Fig. S11), which, as previous described, is associated to an energetic penalty of 1 - 2 kcal mol^{-1} [53]. The ability of Glu363 to adopt different conformations has already been observed by X-ray crystallography, however, few examples are reported [51, 54, 55]. As mentioned before the volume of the active site pocket of nNOS was calculated to be 2203.0 ± 8.3 $Å^3$, while that of eNOS was 2489.0 ± 7.7. The slightly larger and much more open active site of eNOS contrasts with the relatively compact and closed active site topologies of nNOS, which could result in weaker van der Waals interactions between eNOS and **3** (Fig. 10). Such situation could probably account for the worst affinity of **3** toward eNOS.

The MD simulation for **3**:iNOS showed significant changes in the binding conformation of **3** when compared to **3**:nNOS and **3**:eNOS. The molecule bonds to iNOS with the fluorophenyl group less buried in the active site (Fig. 9c). This group is not parallel to the heme plane, as found in nNOS and eNOS, which may account for the decreased potency of **3** toward the iNOS isoform. The aminopyridine moiety extends out of the active site, where it forms a bifurcated hydrogen bridge with heme propionate D and interacts with the peripheral pocket (Met114, Asn115 and Pro116) at the edge of the active site. Comparison of the NOS isoforms structures revealed that Asn115 in iNOS is replaced by Leu337/Leu106 in nNOS/eNOS, respectively, which leads to decreased hydrophobicity in the binding

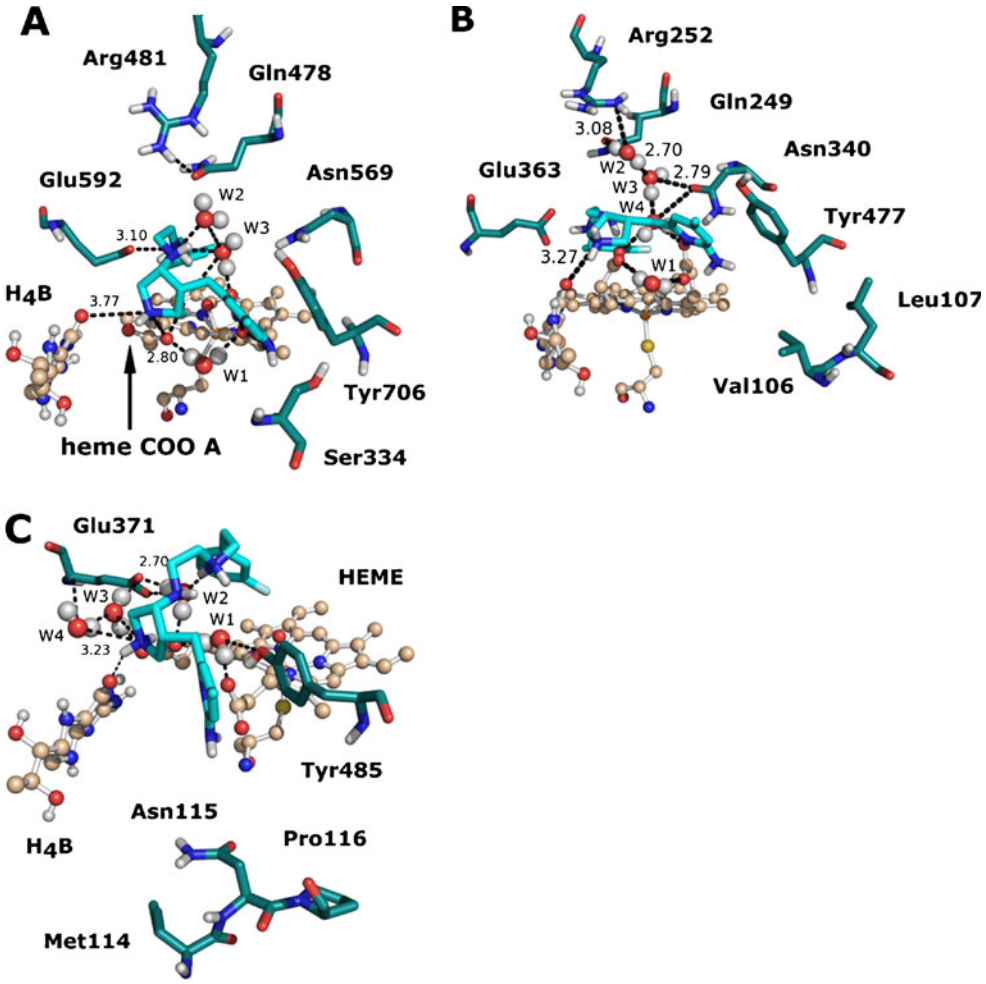

Fig. 9 Structural micro-environment around the active site of the **3**:nNOS (**a**), **3**:eNOS (**b**) and **3**:iNOS (**c**). Inhibitor **3** is shown in cyan sticks

pocket of iNOS, affecting the aminopyridine-protein hydrophobic interaction. The binding mode of **3** in iNOS obtained from the MD simulations correlates well with the analysis of the properties of the iNOS active site. Indeed, as mentioned before, the active site of iNOS is more deeply buried and smaller than the active site of the others isoforms, suggesting that iNOS cannot accommodate large and bulky inhibitors (Fig. 4).

A different pattern of water distribution was found for the isoforms. Water molecules in contact with the inhibitor (within 3 Å) during the last 4 ns of trajectory are shown in Fig. 10. The presence of these water molecules retained at

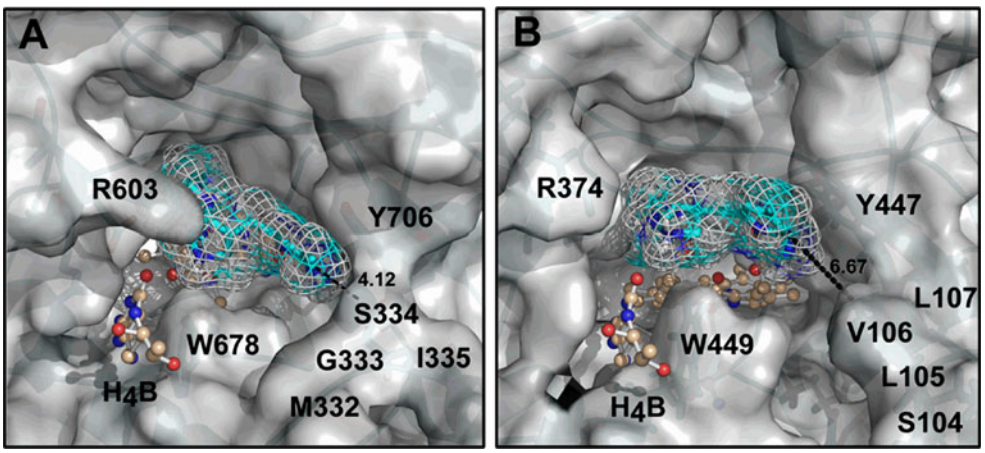

Fig. 10 Surface representation of the "MD binding mode" of **3** in the active site pocket of nNOS (**a**) and eNOS (**b**)

the binding site (residence times between 90 – 100 %) establishing H-bonds to the polar residues can assist the specificity of inhibitor binding. They are occupying well defined sites, acting as an extension of the protein surface, and favoring highly specific interactions with the cavity walls. In complex **3**:iNOS, loss of the π-π stacking interactions between the fluorophenyl and the heme group seems to be compensated by the formation of an extensive network of H-bonds between water molecules, Glu371 and heme propionates (Fig. 9c). It is worth mentioning that even without this π-π interaction, the inhibitory potency of **3** to iNOS (K_i = 3.9 μM) is similar to that found for eNOS (K_i = 20.3 μM), suggesting that these water-mediated interactions are essential for affinity.

In complexes **3**:nNOS and **3**:eNOS "special" water molecules (W2 and W3) absent in **3**:iNOS appear to play important roles in the positioning of the inhibitor (Fig. 9a and b). It is interesting to note that these water molecules, which were seen during the entire last 4 ns of simulation, are also present in the X-ray crystal structures of **3** complexed with nNOS (HOH 1025 and HOH 1029, chain A, PDB ID 3JWT) and eNOS (HOH 1272 and HOH 1270, chain A, PDB ID 3JWX). Both the X-ray crystal structures and the dynamics simulations demonstrate that these water-bridged interactions should be essential to induce the inhibitor to stack against the heme group.

Conclusions

Aiming to rationalize the structural factors responsible for selective inhibition of nitric oxide synthase isoforms, we have performed a detailed MD simulations study. We have selected a well-known inhibitor of NOS with poor isoselectivity (**1**) and potent and highly selective inhibitors of iNOS (**2**) and nNOS (**3**). The application of molecular docking and molecular dynamics simulations enabled a comparative analysis of relevant structural features for which the influence of the atomic and molecular motion is essential. Although in most cases the X-ray crystal structures of a specific inhibitor has shown identical binding modes in the three NOS isoforms, with MD simulations it has been possible to find differences in the binding conformation, and to rationalize the observed isoselectivity.

Despite its low isoselectivity, inhibitor **1** is slightly more selective for nNOS than for the other two isoforms, which can be partially explained by the presence of extra charge–charge interactions. In complex **1**:nNOS, inhibitor **1** adopts an "extended" conformation that allows the -CO_2^- group to be in position to interact with Arg481. The stabilization of this "extended" conformation is explained based on the mutation of Asn498 in nNOS that is Thr277 in iNOS. In fact, the side-chain of Asn498 in nNOS is interacting with Arg481, inducing a rotation in this residue that places its side-chain close to the -CO_2^- group of the inhibitor. In the case of **1**:iNOS the inhibitor adopts a "curled" conformation, which results in electrostatic repulsions observed between its CO_2^- group and Asp376 justifying the low affinity of **1** for this isoform. In the case of **1**:eNOS, the "curled" conformation of the inhibitor is stabilized by Asn368, which is Asp376 in iNOS. The lack of electrostatic repulsions in eNOS accounts for the better selectivity of **1** toward eNOS over iNOS.

MD simulations of inhibitor **2** bound to iNOS and nNOS showed that its binding conformation is similar in both isoforms. The 80-fold selectivity for iNOS over nNOS observed experimentally for **2** can be rationalized in terms of the greater hydrophobic and cation-π interactions of the cyanophenyl group with Arg260 and Arg382 in iNOS isoform. In fact, the selectivity should be related with the ability of Gln257 to switch between "open" and "closed" conformations, with the appearance of an iNOS-specific subpocket composed by Gln257, Arg260 and Arg382. The inhibitor-heme π-stacking interactions observed in **2**:iNOS and **2**:nNOS are not observed in complex **2**:eNOS, which may account for the lower affinity of **2** for eNOS. Moreover, the inhibitor binding induced a conformational change in Glu363 that was reported to be associated to an energetic penalty of 1 – 2 kcal.

The molecular recognition pattern within the tree isoforms is consistent with the higher affinity of inhibitor **3** to nNOS over the other two isoforms. For the complex **3**:eNOS, our simulation results revealed that the side chain of Glu363 also adopts an alternate conformation, similar to what happens in **2**:eNOS. Owing to the more closed and compact active site of nNOS (compared to eNOS) stronger van der Waals interactions were observed between **3** and nNOS, which may also account for its better affinity for this isoform. In the case of **3**:iNOS, the elongated and narrow binding pocket of this isoform does not allow the positioning of the inhibitor over the heme group, and, in this way, the π-π interactions observed for nNOS and eNOS between the fluorophenyl group of **3** and the porphyrin ring of the heme group are lost. Water-bridged H-bonds between the nNOS and eNOS isoforms and the inhibitor **3** appear to facilitate the stacking of the latter against the heme group.

Brought together, the results suggest that compounds with an elongated shape present higher selectivity for iNOS. Indeed, due to the narrow and buried binding pocket of this isoform, a potent and selective inhibitor should have a "cylindrical-like shape" similar to inhibitor **2**. Additionally, the presence of hydrophobic and aromatic tails capable of interacting with the iNOS-specific subpocket created by Gln257 is also essential. nNOS isoform selectivity may be achieved by using inhibitors with hydrophobic and aromatic tail containing amine groups that reach the substrate access channel and interact with the heme propionate D, the non-conserved hydrophobic pocket formed by Ser334, Met336,

Leu337 and Pro338, and the conserved Tyr706 residue. These findings may offer valuable hints for the design of NOS inhibitors with improved isoselectivity and potency.

Acknowledgments This work has been partially supported by the Fundação para a Ciência e Tecnologia (FCT), Portugal (PTDC/QUI-QUI/121752/2010). We would like to thank F.-Y. Dupradeau for advice on using the R.E.D. server and for helpful discussions.

References

1. Alderton WK, Cooper CE, Knowles RG (2001) Nitric oxide synthases: structure, function and inhibition. Biochem J 357:593–615
2. Moncada S, Palmer RM, Higgs EA (1991) Nitric oxide: physiology, pathophysiology, and pharmacology. Pharmacol Rev 43 (2):109–142
3. Li H, Poulos TL (2005) Structure-function studies on nitric oxide synthases. J Inorg Biochem 99(1):293–305
4. Leiper J, Nandi M (2011) The therapeutic potential of targeting endogenous inhibitors of nitric oxide synthesis. Nat Rev Drug Discov 10(4):277–291
5. Ji H, Erdal EP, Litzinger EA, Seo J, Zhu Y, Xue F, Fang J, Huang J, Silverman RB (2009) Selective neuronal nitric oxide synthase inhibitors. Front Med Chem 4:842–882
6. Wink DA, Mitchell JB (2003) Nitric oxide and cancer: an introduction. Free Radic Biol Med 34(8):951–954
7. Huang PL, Huang Z, Mashimo H, Bloch KD, Moskowitz MA, Bevan JA, Fishman MC (1995) Hypertension in mice lacking the gene for endothelial nitric oxide synthase. Nature 377(6546):239–242
8. Vallance P, Leiper J (2002) Blocking NO synthesis: how, where and why? Nat Rev Drug Discov 1(12):939–950
9. Di Giacomo C, Sorrenti V, Salerno L, Cardile V, Guerrera F, Siracusa MA, Avitabile M, Vanella A (2003) Novel inhibitors of neuronal nitric oxide synthase. Exp Biol Med 228(5):486–490
10. Zicha J, Pechánová O, Dobesová Z, Kunes J (2003) Hypertensive response to chronic NG-nitro-L-arginine methyl ester (L-NAME) treatment is similar in immature and adult Wistar rats. Clin Sci 105 (4):483–489
11. Macdonald JE (1996) Chapter 23. Nitric oxide synthase inhibitors. Ann Rep Med Chem 31:221–230
12. Granik VG, Grigorev NB (2002) Nitric oxide synthase inhibitors: biology and chemistry. Russ Chem Bull 51(11):1973–1995
13. Tafi A, Angeli L, Venturini G, Travagli M, Corelli F, Botta M (2006) Computational studies of competitive inhibitors of nitric oxide synthase (NOS) enzymes: towards the development of powerful and isoform-selective inhibitors. Curr Med Chem 13 (16):1929–1946
14. Oliveira BL, Correia JDG, Raposinho PD, Santos I, Ferreira A, Cordeiro C, Freire AP (2009) Re and 99mTc organometallic complexes containing pendant l-arginine derivatives as potential probes of inducible nitric oxide synthase. Dalton Trans 1:152–162
15. Oliveira BL, Raposinho PD, Mendes F, Figueira FV, Santos I, Ferreira AN, Cordeiro C, Freire AP, Correia JDG (2010) Re and Tc tricarbonyl complexes: from the suppression of NO biosynthesis in macrophages to in vivo targeting of inducible nitric oxide synthase. Bioconjug Chem 21(12):2168–2172
16. Oliveira BL, Raposinho PD, Mendes F, Santos IC, Santos I, Ferreira A, Cordeiro C, Freire AP, Correia JDG (2011) Targeting nitric oxide synthase with 99mTc/Re-tricarbonyl complexes containing pendant guanidino or isothiourea moieties. J Organomet Chem 696(5):1057–1065
17. Fischmann TO, Hruza A, Niu XD, Fossetta JD, Lunn CA, Dolphin E, Prongay AJ, Reichert P, Lundell DJ, Narula SK, Weber PC (1999) Structural characterization of nitric oxide synthase isoforms reveals striking active-site conservation. Nat Struct Mol Biol 6 (3):233–242
18. Garvey EP, Oplinger JA, Furfine ES, Kiff RJ, Laszlo F, Whittle BJR, Knowles RG (1997) 1400W Is a slow, tight binding, and highly selective inhibitor of inducible nitric-oxide synthase in vitro and in vivo. J Biol Chem 272(8):4959–4963
19. Fedorov R, Hartmann E, Ghosh DK, Schlichting I (2003) Structural basis for the specificity of the nitric-oxide synthase inhibitors W1400 and Nω-Propyl-l-Arg for the inducible and neuronal isoforms. J Biol Chem 278(46):45818–45825
20. Li H, Raman CS, Martásek P, Masters BSS, Poulos TL (2001) Crystallographic studies on endothelial nitric oxide synthase complexed with nitric oxide and mechanism-based inhibitors†. Biochemistry 40(18):5399–5406
21. Ji H, Stanton BZ, Igarashi J, Li H, Martásek P, Roman LJ, Poulos TL, Silverman RB (2008) Minimal pharmacophoric elements and fragment hopping, an approach directed at molecular diversity and isozyme selectivity. Design of selective neuronal nitric oxide synthase inhibitors. J Am Chem Soc 130(12):3900–3914
22. Garcin ED, Arvai AS, Rosenfeld RJ, Kroeger MD, Crane BR, Andersson G, Andrews G, Hamley PJ, Mallinder PR, Nicholls DJ, St-Gallay SA, Tinker AC, Gensmantel NP, Mete A, Cheshire DR, Connolly S, Stuehr DJ, Aberg A, Wallace AV, Tainer JA, Getzoff ED (2008) Anchored plasticity opens doors for selective inhibitor design in nitric oxide synthase. Nat Chem Biol 4 (11):700–707
23. Matter H, Kumar HSA, Fedorov R, Frey A, Kotsonis P, Hartmann E, Fröhlich LG, Reif A, Pfleiderer W, Scheurer P, Ghosh DK, Schlichting I, Schmidt HHHW (2005) Structural analysis of isoform-specific inhibitors targeting the tetrahydrobiopterin binding site of human nitric oxide synthases. J Med Chem 48 (15):4783–4792
24. Li H, Raman CS, Martásek P, Král V, Masters BSS, Poulos TL (2000) Mapping the active site polarity in structures of endothelial nitric oxide synthase heme domain complexed with isothioureas. J Inorg Biochem 81(3):133–139
25. Morris GM, Goodsell DS, Halliday RS, Huey R, Hart WE, Belew RK, Olson AJ (1998) Automated docking using a Lamarckian genetic algorithm and an empirical binding free energy function. J Comput Chem 19(14):1639–1662
26. Morris GM, Huey R, Lindstrom W, Sanner MF, Belew RK, Goodsell DS, Olson AJ (2009) AutoDock4 and AutoDockTools4: automated docking with selective receptor flexibility. J Comput Chem 30(16):2785–2791
27. Shelley J, Cholleti A, Frye L, Greenwood J, Timlin M, Uchimaya M (2007) Epik: a software program for pKa prediction and protonation state generation for drug-like molecules. J Comput Aided Mol Des 21(12):681–691
28. Bayly CI, Cieplak P, Cornell W, Kollman PA (1993) A well-behaved electrostatic potential based method using charge restraints for deriving atomic charges: the RESP model. J Phys Chem 97(40):10269–10280
29. Cornell WD, Cieplak P, Bayly CI, Kollmann PA (1993) Application of RESP charges to calculate conformational energies, hydrogen bond energies, and free energies of solvation. J Am Chem Soc 115(21):9620–9631
30. Dupradeau F-Y, Pigache A, Zaffran T, Savineau C, Lelong R, Grivel N, Lelong D, Rosanski W, Cieplak P (2010) The R.E.D. tools: advances in RESP and ESP charge derivation and force field library building. Phys Chem Chem Phys 12(28):7821–7839
31. Vanquelef E, Simon S, Marquant G, Garcia E, Klimerak G, Delepine JC, Cieplak P, Dupradeau F-Y (2011) R.E.D. Server: a web service for deriving RESP and ESP charges and building force

field libraries for new molecules and molecular fragments. Nucleic Acids Res 39(suppl 2):W511–W517
32. Dupradeau F-Y, Cézard C, Lelong R, Stanislawiak É, Pêcher J, Delepine JC, Cieplak P (2008) R.E.DD.B.: a database for RESP and ESP atomic charges, and force field libraries. Nucleic Acids Res 36(suppl 1):D360–D367
33. Vanommeslaeghe K, Hatcher E, Acharya C, Kundu S, Zhong S, Shim J, Darian E, Guvench O, Lopes P, Vorobyov I, Mackerell AD (2010) CHARMM general force field: a force field for drug-like molecules compatible with the CHARMM all-atom additive biological force fields. J Comput Chem 31(4):671–690
34. Li H, Raman CS, Glaser CB, Blasko E, Young TA, Parkinson JF, Whitlow M, Poulos TL (1999) Crystal structures of zinc-free and -bound heme domain of human inducible nitric-oxide synthase. J Biol Chem 274(30):21276–21284
35. Phillips JC, Braun R, Wang W, Gumbart J, Tajkhorshid E, Villa E, Chipot C, Skeel RD, Kalé L, Schulten K (2005) Scalable molecular dynamics with NAMD. J Comput Chem 26(16):1781–1802
36. MacKerell AD, Bashford D, Bellott, Dunbrack RL, Evanseck JD, Field MJ, Fischer S, Gao J, Guo H, Ha S, Joseph-McCarthy D, Kuchnir L, Kuczera K, Lau FTK, Mattos C, Michnick S, Ngo T, Nguyen DT, Prodhom B, Reiher WE, Roux B, Schlenkrich M, Smith JC, Stote R, Straub J, Watanabe M, Wiorkiewicz-Kuczera J, Yin D, Karplus M (1998) All-atom empirical potential for molecular modeling and dynamics studies of proteins. J Phys Chem B 102(18):3586–3616
37. Humphrey W, Dalke A, Schulten K (1996) VMD: visual molecular dynamics. J Mol Graph 14(1):33–38
38. Cho K-B, Derat E, Shaik S (2007) Compound I of nitric oxide synthase: the active site protonation state. J Am Chem Soc 129(11):3182–3188
39. Dolinsky TJ, Nielsen JE, McCammon JA, Baker NA (2004) PDB2PQR: an automated pipeline for the setup of Poisson–Boltzmann electrostatics calculations. Nucleic Acids Res 32(suppl 2):W665–W667
40. Dolinsky TJ, Czodrowski P, Li H, Nielsen JE, Jensen JH, Klebe G, Baker NA (2007) PDB2PQR: expanding and upgrading automated preparation of biomolecular structures for molecular simulations. Nucleic Acids Res 35(suppl 2):W522–W525
41. Li H, Robertson AD, Jensen JH (2005) Very fast empirical prediction and rationalization of protein pKa values. Proteins Struct Funct Bioinforma 61(4):704–721
42. Essmann U, Perera L, Berkowitz ML, Darden T, Lee H, Pedersen LG (1995) A smooth particle mesh Ewald method. J Chem Phys 103(19):8577–8593
43. Hoover WG (1985) Canonical dynamics: equilibrium phase-space distributions. Phys Rev A 31(3):1695
44. Feller SE, Zhang Y, Pastor RW, Brooks BR (1995) Constant pressure molecular dynamics simulation: the Langevin piston method. J Chem Phys 103(11):4613–4621
45. Nosé S (2002) A molecular dynamics method for simulations in the canonical ensemble. Mol Phys Int J Interface Chem Phys 100 (1):191–198
46. Grest GS, Kremer K (1986) Molecular dynamics simulation for polymers in the presence of a heat bath. Phys Rev A 33(5):3628
47. DeLano WL (2002) The PyMOL molecular graphics system. DeLano Scientific, San Carlos
48. Volarea. João Ribeiro, Group of Computational BioChemistry, Faculty of Sciences of the University of Porto, Porto, Portugal, http://www.compbiochem.org/Software/Volarea/Home.html
49. Coleman RG, Sharp KA (2006) Travel depth, a new shape descriptor for macromolecules: application to ligand binding. J Mol Biol 362(3):441–458
50. Dijkstra EW (1959) A note on two problems in connexion with graphs. Numer Math 1(1):269–271
51. Delker SL, Ji H, Li H, Jamal J, Fang J, Xue F, Silverman RB, Poulos TL (2010) Unexpected binding modes of nitric oxide synthase inhibitors effective in the prevention of a cerebral palsy phenotype in an animal model. J Am Chem Soc 132(15):5437–5442
52. Aparna V, Desiraju GR, Gopalakrishnan B (2007) Insights into ligand selectivity in nitric oxide synthase isoforms: a molecular dynamics study. J Mol Graph Model 26(2):457–470
53. Rosenfeld RJ, Garcin ED, Panda K, Andersson G, Åberg A, Wallace AV, Morris GM, Olson AJ, Stuehr DJ, Tainer JA, Getzoff ED (2002) Conformational changes in nitric oxide synthases induced by chlorzoxazone and nitroindazoles: crystallographic and computational analyses of inhibitor potency. Biochemistry 41(47):13915–13925
54. Xue F, Li H, Delker SL, Fang J, Martasek P, Roman LJ, Poulos TL, Silverman RB (2010) Potent, highly selective, and orally bioavailable Gem-difluorinated monocationic inhibitors of neuronal nitric oxide synthase. J Am Chem Soc 132 (40):14229–14238
55. Ji H, Delker SL, Li H, Martasek P, Roman LJ, Poulos TL, Silverman RB (2010) Exploration of the active site of neuronal nitric oxide synthase by the design and synthesis of pyrrolidinomethyl 2-aminopyridine derivatives. J Med Chem 53(21):7804–7824